

# Influence of the chiral magnetic effect on particle-pair elliptic anisotropy

Han-Sheng Li,<sup>1,\*</sup> Yicheng Feng,<sup>1,†</sup> and Fuqiang Wang<sup>1,2,‡</sup>

<sup>1</sup>*Department of Physics and Astronomy, Purdue University, West Lafayette, IN 47907, USA*

<sup>2</sup>*School of Science, Huzhou University, Huzhou, Zhejiang 313000, China*

Chiral Magnetic Effect (CME) is a phenomenon in which electric charge is separated by a strong magnetic field from local domains of chirality imbalance in quantum chromodynamics. The CME-sensitive, azimuthal correlator difference  $\Delta\gamma$  between opposite-sign (OS) and same-sign (SS) charged hadron pairs is contaminated by a major physics background proportional to the particle elliptic anisotropy ( $v_2$ ). The CME signal, on the other hand, contributes to the difference in the pair elliptic anisotropies between OS and SS pairs ( $\Delta v_{2,\text{pair}}$ ). We investigate  $\Delta v_{2,\text{pair}}$  and found its sensitivity to CME to be similar to that of the  $\Delta\gamma$  observable.

## I. INTRODUCTION

One of the unsettled questions in relativistic heavy ion collisions is the chiral magnetic effect (CME). It is predicted by quantum chromodynamics (QCD) to exist because of vacuum fluctuations of topological charges, yielding a chirality imbalance of quarks in local domains and subsequent charge separations under a strong magnetic field [1–4]. Such a strong magnetic field is presumably produced in non-head-on relativistic heavy ion collisions [5, 6]. However, definite signals of the CME have not yet been observed [7, 8].

The magnetic field created in heavy ion collisions is on average perpendicular to the reaction plane (RP, the plane spanned by the beam and the impact parameter direction of the collision). The CME charge separation signal is an excess of particles of one charge sign perpendicular to the RP and of the opposite charge sign in the opposite direction [3]. It is convenient to express it in Fourier series [9],

$$dN_{\pm}/d\phi \propto 1 + 2v_2 \cos 2\phi \pm 2a_1 \sin \phi + \dots, \quad (1)$$

where  $\phi$  is the azimuthal angle of the particle momentum vector with respect to RP and the subscript  $\pm$  indicates particle charge sign. Because of random fluctuations of the vacuum topological charge sign, the CME signal parameter  $a_1$  is also random in sign, rendering a vanishing average signal on single particle level [2]. The commonly used observable is thus a two-particle correlator [9],

$$\gamma = \langle \cos(\phi_{\alpha} + \phi_{\beta}) \rangle, \quad (2)$$

where  $\phi_{\alpha}$  and  $\phi_{\beta}$  are the azimuthal angles of two particles of interest (POI). Because of the presence of charge-independent background, such as effects from global momentum conservation, the difference between opposite-sign (OS) and same-sign (SS) correlators is used in experimental search for the CME [9],

$$\Delta\gamma \equiv \gamma_{\text{os}} - \gamma_{\text{ss}}. \quad (3)$$

The CME signal presented in the  $\Delta\gamma$  observable is  $2a_1^2$ . However, charge-dependent background is also present in the  $\Delta\gamma$  correlator, such as correlations between daughter particles from a resonance decay, or among particles from the same jet or a back-to-back dijet [9–12]. This background correlation can be schematically expressed as [9]

$$\Delta\gamma_{\text{res}} = \langle \cos(\phi_{\alpha} + \phi_{\beta}) \rangle v_{2,\text{res}}, \quad (4)$$

where the subscript "res" stands generically for genuine two-particle correlations such as those due to resonance decays and jets, and  $v_{2,\text{res}} \equiv \langle \cos 2\phi_{\text{res}} \rangle$  is the elliptic flow anisotropy of those two-particle correlation clusters.

The charge-dependent background turns out to be significant [12], and can nearly explain the measured  $\Delta\gamma$  magnitude [13, 14]. Large efforts have since been investigated to eliminate or mitigate this background [15–19], including innovative observables [20–23].

Although the CME is a parity-odd phenomenon, the two-particle  $\Delta\gamma$  correlator observable is intrinsically parity even. As a result, the CME signal will appear as a component in the pair-wise elliptic anisotropies ( $v_{2,\text{pair}}$ ). It has been recently pointed out by Ref. [24] that resonance  $v_{2,\text{res}}$  and particle pair  $v_{2,\text{pair}}$  contain CME information and should in principle be able to probe the CME as well. In this article, we follow up on this point and investigate further insights, if any, that pair  $v_{2,\text{pair}}$  may bring to the CME search endeavor.

## II. AVFD SIMULATION

We use the Anomalous-Viscous Fluid Dynamics (AVFD) model [25–27] for our investigation. AVFD is an anomalous fluid dynamics developed to describe the evolution of chiral fermion currents in the quark-gluon plasma (QGP) created in relativistic heavy ion collisions in addition to the normal VISHNU simulations [28]. The average magnetic field can be calculated from the spectator protons and it is along the direction perpendicular to RP. In the model, the magnetic field is quantified by event-by-event simulations [29] taking into account the fluctuations of the magnetic field direction with respect

\* li3924@purdue.edu

† feng216@purdue.edu

‡ fqwang@purdue.edu

to the RP. A modest time evolution is assumed for the decreasing magnetic field with a typical lifetime comparable to the initial time of hydrodynamic evolution  $\sim 0.6$  fm/c. The initial condition for the axial charge density ( $n_5$ ) is dynamically generated in AVFD to be proportional to the entropy density ( $s$ ), and the strength is set via the proportionality coefficient  $n_5/s$ . The QGP medium evolution is simulated by viscous hydrodynamics to describe the bulk background in heavy ion collisions, with transport parameters for the diffusion coefficient as well as the relaxation time. A final hadronic stage after the hydrodynamic freeze-out is included with hadronic re-scatterings and resonance decays.

Au+Au collisions at 200 GeV were simulated by AVFD. In this study we focus on the centrality range of 30-40% [30]. Three  $n_5/s$  values are used in the simulations,  $n_5/s=0$ , 0.1, and 0.2. Each of these simulations has around 20M events generated.

In the analysis of this work, the RP is taken from the simulation, fixed to zero. The POI's are taken to be within the acceptance of  $|\eta| < 1$  and  $0.2 < p_T < 2$  GeV/c, typical of midrapidity detectors such as the STAR experiment [31].

### III. RESONANCE ELLIPTIC ANISOTROPIES

We examine the invariant mass ( $m_{\text{inv}}$ ) distributions of charged hadron pairs in this study. Figure 1 upper panel shows the OS and SS pair  $m_{\text{inv}}$  distributions, assuming pion mass for all hadrons, from AVFD simulation with  $n_5/s = 0$  as an example. The lower panel of Fig. 1 shows the difference of the  $m_{\text{inv}}$  distributions between OS and SS pairs for all three  $n_5/s$  values. The CME implemented in AVFD affects the relative OS and SS pair  $m_{\text{inv}}$  distributions—the distribution flattens with larger  $n_5/s$ . This arises from contributions from back-to-back OS pairs (hence larger  $m_{\text{inv}}$ ) and near-side SS pairs (hence smaller  $m_{\text{inv}}$ ), resulting in an enhancement at large  $m_{\text{inv}}$  and depletion at small  $m_{\text{inv}}$  for large  $n_5/s$  compared to small one.

Several resonance peaks are apparent in the  $m_{\text{inv}}$  distributions,  $\rho$ ,  $f_0(980)$ , and  $f_2(1270)$ . No intrinsic mass width is implemented in AVFD, so the resonances appear as sharp peaks. It is interesting to investigate the  $v_{2,\text{res}}$  of those resonances, which can be obtained from elliptic anisotropies of OS pairs ( $v_{2,\text{os}}$ ) and SS pairs ( $v_{2,\text{ss}}$ ). We focus on the  $\rho$  resonance here. The  $v_{2,\text{os}}$  and  $v_{2,\text{ss}}$  are shown in Fig. 2 as functions of  $m_{\text{inv}}$  in the vicinity of the  $\rho$  resonance peak for the three  $n_5/s$  cases.

In Ref. [24] the resonance  $v_{2,\text{res}}$  is calculated, after applying a  $m_{\text{inv}}$  window, by

$$v_{2,\text{res}} = \frac{N_{\text{os}} \langle \cos 2\phi_{\text{os}} \rangle - N_{\text{ss}} \langle \cos 2\phi_{\text{ss}} \rangle}{N_{\text{os}} - N_{\text{ss}}}. \quad (5)$$

This would work if  $v_{2,\text{os}}$  and  $v_{2,\text{ss}}$  are equal and  $N_{\text{ss}}$  represents the true number of background pairs underneath the resonance peak of  $N_{\text{os}}$  pairs. Neither of these two

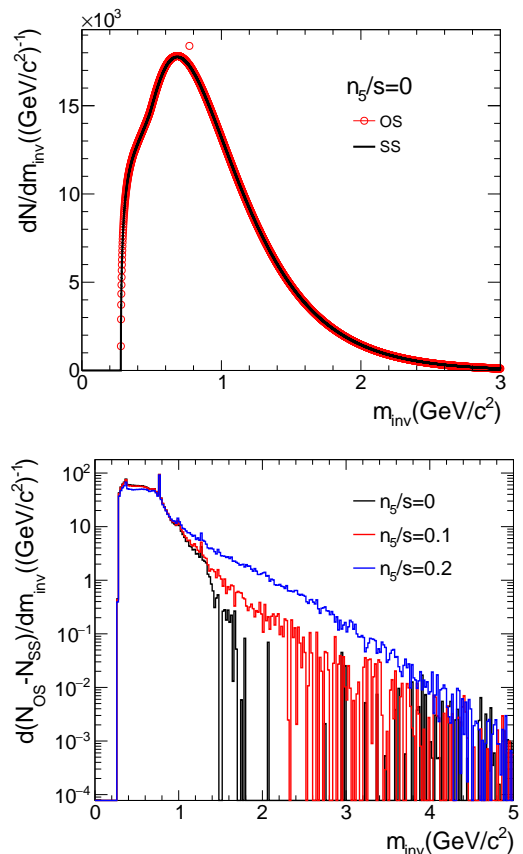


FIG. 1. (Upper panel) Invariant mass ( $m_{\text{inv}}$ ) distributions of opposite-sign (OS) pairs and same-sign (SS) pairs simulated by AVFD with axial current density of  $n_5/s = 0$ . Pion mass is assumed for all charged particles in calculating  $m_{\text{inv}}$ . (Lower panel) Difference in the  $m_{\text{inv}}$  distributions of OS and SS pairs from AVFD simulations with  $n_5/s = 0, 0.1, \text{ and } 0.2$ .

conditions is valid as seen from Figs. 1 and 2. Thus, the calculated  $v_{2,\text{res}}$  by Eq. 5 would be incorrect. This is particularly so if a wide  $m_{\text{inv}}$  window is applied to embrace the resonance peak, as shown in filled markers in Fig. 3 for the  $\rho$  resonance as an example. The calculated  $v_{2,\text{res}}$  increases with  $n_5/s$  because of an increasing departure between  $v_{2,\text{os}}$  and  $v_{2,\text{ss}}$ . With a narrow mass window, the issue becomes less significant but non-vanishing as indicated by the open circles in Fig. 3.

Often resonance  $v_{2,\text{res}}$  is analyzed by the so-called invariant mass method [32], where the  $\langle \cos 2\phi \rangle$  is calculated as a function of  $m_{\text{inv}}$ , and a fit is performed taking into account the  $m_{\text{inv}}$  dependence of the resonance signal to background ratio and assuming a background  $v_2$  dependence on  $m_{\text{inv}}$  (typically a first- or second-order polynomial). In this case, only the OS information are needed. We calculate the  $v_{2,\text{res}}$  in the same spirit as the invariant mass method, namely by scaling the SS quantities up to match the OS's,

$$v_{2,\text{res}} = \frac{N_{\text{os}} \langle \cos 2\phi_{\text{os}} \rangle - r_N r_{v_2} N_{\text{ss}} \langle \cos 2\phi_{\text{ss}} \rangle}{N_{\text{os}} - r_N N_{\text{ss}}}. \quad (6)$$

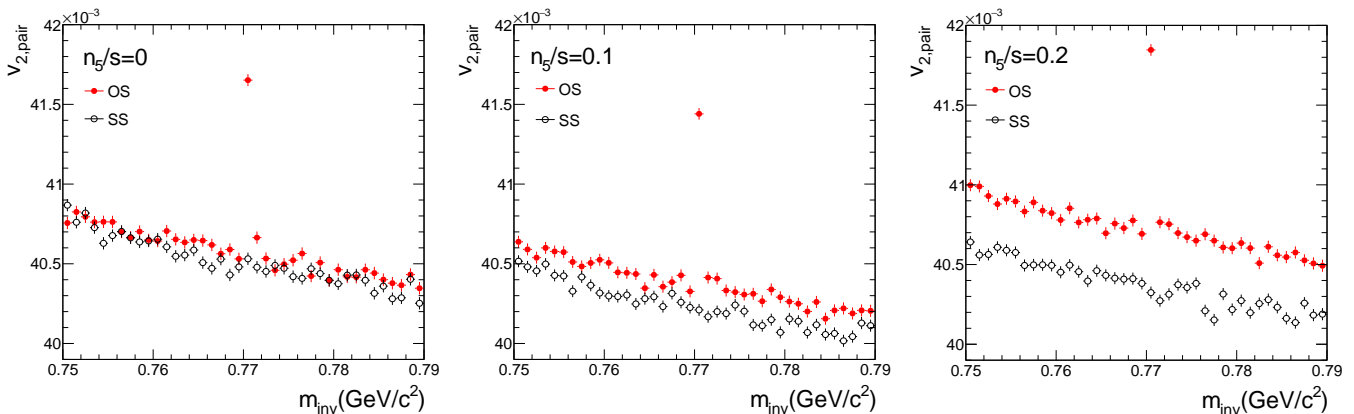


FIG. 2. Elliptic anisotropies  $v_{2,\text{pair}}$  of OS and SS pairs with respect to the known impact parameter direction as functions of  $m_{\text{inv}}$ , simulated by AVFD for  $n_5/s = 0$  (left panel), 0.1 (center panel), and 0.2 (right panel).

Here,  $r_N$  is the scaling factor to scale the SS multiplicity up to that of OS's, and  $r_{v_2}$  is that to scale  $v_{2,\text{ss}}$  up to match  $v_{2,\text{os}}$  in the non-resonance (sideband) regions. The obtained  $v_{2,\text{res}}$  is shown by the red squares in Fig. 3. The  $v_{2,\rho}$  appears to be constant over  $n_5/s$ , suggesting that influences from the CME on resonance elliptic anisotropies, if any, are small.

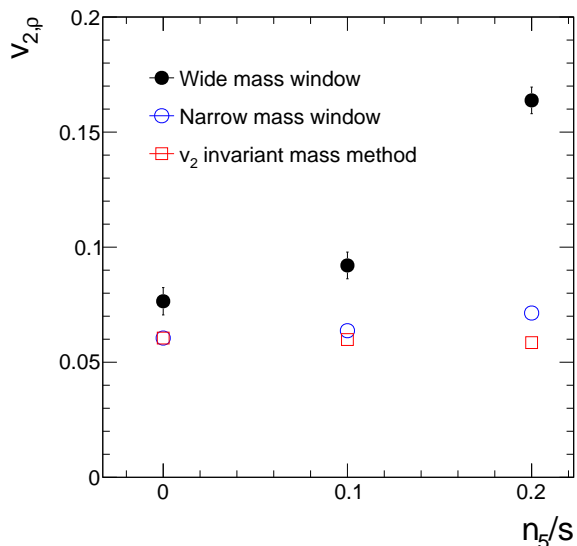


FIG. 3. The  $\rho$  resonance  $v_{2,\rho}$  calculated by Eq. (5) with a wide mass window  $0.765 < m_{\text{inv}} < 0.785 \text{ GeV}/c^2$  (blue points) and a narrow mass window  $0.769 < m_{\text{inv}} < 0.772 \text{ GeV}/c^2$  (black points), plotted vs.  $n_5/s$ . The  $v_{2,\rho}$  calculated by Eq. (6) is shown in red markers.

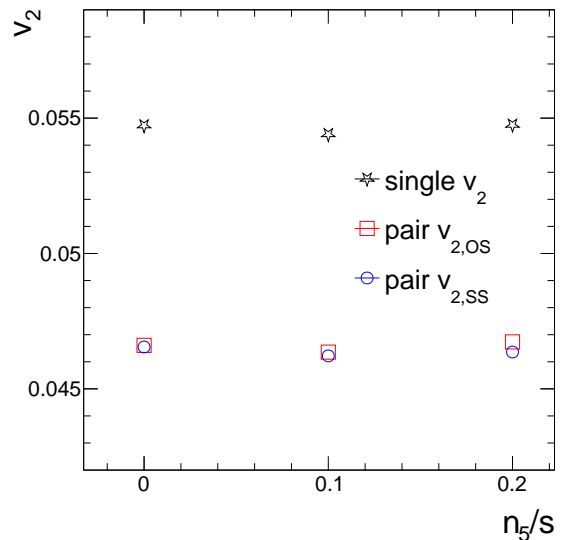


FIG. 4. Pair anisotropy  $v_{2,\text{os}}$  and  $v_{2,\text{ss}}$  as functions of  $n_5/s$ , together with single particle  $v_2$ .

#### IV. PAIR ELLIPTIC ANISOTROPY DIFFERENCE

It is interesting to notice that the splitting between  $v_{2,\text{os}}$  and  $v_{2,\text{ss}}$  in Fig. 3 increases with increasing  $n_5/s$ . This is observed also in the entire region of  $m_{\text{inv}}$  as shown in Fig. 5. In other words, the CME in AVFD leaves an imprint in this split. This has been pointed out by Ref. [24]. It is therefore interesting to examine this split. To this end, we first obtain the pair  $v_{2,\text{os}}$  and  $v_{2,\text{ss}}$  averaged over the entire  $m_{\text{inv}}$  range. These are shown in Fig. 4. For comparison, the single particle  $v_2$  is also shown in Fig. 4.

To gain further insights, we make approximations to analytically examine the pair  $v_{2,\text{pair}}$ , following Ref. [24].

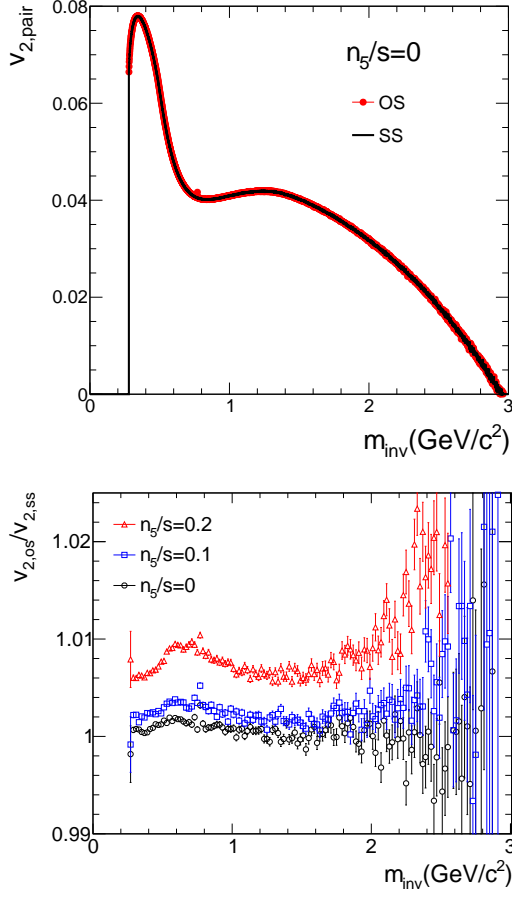


FIG. 5. (Upper panel) Elliptic anisotropies  $v_{2,\text{pair}}$  of OS and SS pairs with respect to the known impact parameter direction as a function of  $m_{\text{inv}}$  over a wide range in  $m_{\text{inv}}$ , simulated by AVFD for  $n_5/s = 0$ . (Lower panel) Ratio of OS and SS pair elliptic anisotropies,  $v_{2,\text{os}}/v_{2,\text{ss}}$ , as functions of  $m_{\text{inv}}$ .

The pair elliptic anisotropy is by definition,

$$v_{2,\text{pair}} = \left\langle \frac{(p_{x,\alpha} + p_{x,\beta})^2 - (p_{y,\alpha} + p_{y,\beta})^2}{(p_{x,\alpha} + p_{x,\beta})^2 + (p_{y,\alpha} + p_{y,\beta})^2} \right\rangle, \quad (7)$$

where pairs can be distinguished between OS and SS pairs. For equal  $p_T$  pairs and under certain assumptions, it may be expressed into [24]

$$v_{2,\text{pair}} = \left\langle \frac{(\cos 2\phi_\alpha + \cos 2\phi_\beta)/2 + \cos(\phi_\alpha + \phi_\beta)}{1 + \cos(\phi_\alpha - \phi_\beta)} \right\rangle \approx v_2(1 - \delta) + \gamma. \quad (8)$$

From this approximation, the dominant component in  $v_{2,\text{pair}}$  appears to be the single particle  $v_2$ . Indeed, this is the case from AVFD simulation, as shown in Fig. 4. The difference between  $v_{2,\text{pair}}$  and  $v_2$  from the approximation is on the order of  $\gamma$  and  $v_2\delta$ . For reference, we show in Fig. 6 the  $\gamma$  and  $\delta$  quantities from the AVFD simulation. The  $\gamma$  and  $\delta$  are significantly smaller than the differences observed between  $v_{2,\text{pair}}$  and  $v_2$ , so quantitatively, Eq. 8 cannot describe  $v_{2,\text{pair}}$ . This can be understood because gross assumptions are made in deriving Eq. 8. For instance, for equal  $p_T$  pairs, the  $v_{2,\text{pair}}$  would simply be  $\langle \cos(\alpha + \beta) \rangle$  which is the  $\gamma$  variable weighted by equal- $p_T$  pair probabilities.

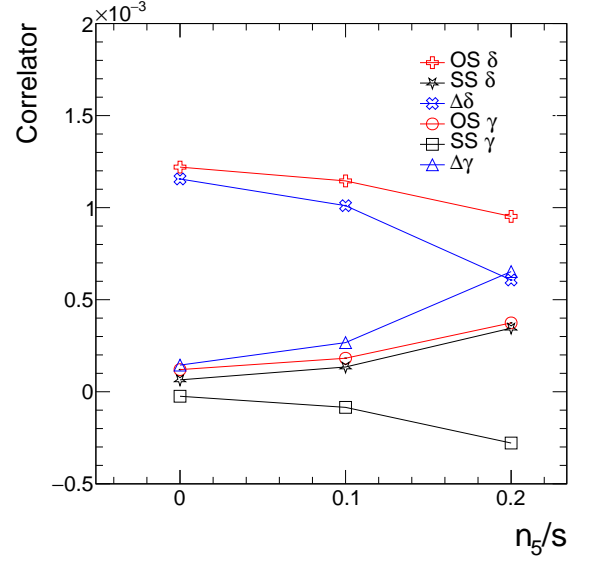


FIG. 6. Calculated  $\gamma$  and  $\delta$  correlators for OS and SS pairs and the corresponding  $\Delta\gamma$  and  $\Delta\delta$  correlators as functions of  $n_5/s$  by AVFD.

We are interested in the  $v_2$  split between OS and SS pairs,

$$\Delta v_{2,\text{pair}} \equiv v_{2,\text{os}} - v_{2,\text{ss}}. \quad (9)$$

Fig. 7 shows  $\Delta v_{2,\text{pair}}$  as a function of  $n_5/s$  in filled circles. An increase in  $\Delta v_{2,\text{pair}}$  with  $n_5/s$  is observed. The red curve is a quadratic fit to  $\Delta v_{2,\text{pair}}$ , which describes  $\Delta v_{2,\text{pair}}$  well, suggesting that  $\Delta v_{2,\text{pair}}$  is sensitive to CME. The nonzero  $\Delta v_{2,\text{pair}}$  at  $n_5/s = 0$  suggests a background contribution to  $\Delta v_{2,\text{pair}}$ .

From the approximation of Eq. 8, one can obtain

$$\Delta v_{2,\text{pair}} \approx \Delta\gamma - v_2\Delta\delta \approx 2a_1^2(1 + v_2) + \frac{N_{\text{res}}}{N_{\text{os}}} [\langle \cos(\phi_\alpha + \phi_\beta - 2\phi_{\text{res}}) \rangle v_{2,\text{res}} - \langle \cos(\phi_\alpha - \phi_\beta) \rangle_{\text{res}} v_2]. \quad (10)$$

It appears to be sensitive to both  $\Delta\gamma$  and  $\Delta\delta$ , containing

contributions from the CME and background. For com-

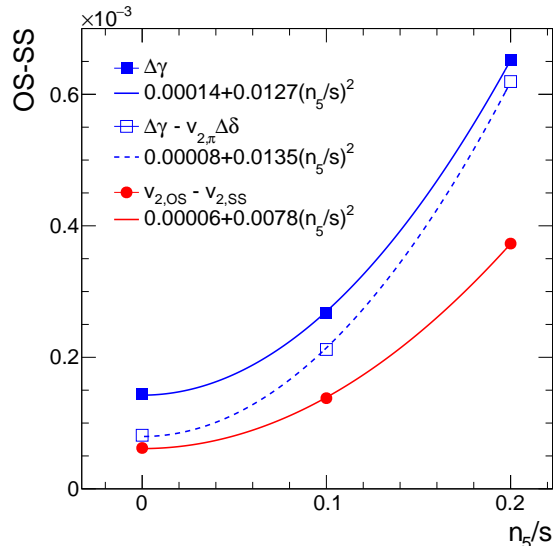


FIG. 7. Pair anisotropy difference  $\Delta v_{2,\text{pair}} \equiv v_{2,\text{os}} - v_{2,\text{ss}}$  as functions of  $n_5/s$ , together with  $\Delta\gamma$  and  $\Delta\gamma - v_{2,\pi}\Delta\delta$ . The  $n_5/s = 0$  data are pure background, while at  $n_5/s=0.1$  and  $0.2$  both CME signal and background are present.

parison, we superimpose  $\Delta\gamma - v_{2,\pi}\Delta\delta$  in Fig. 7 in open squares. Again the data points can not be quantitatively described by Eq. 10 because of the assumptions made in deriving the equations, but the agreement is better than for the individual  $v_{2,\text{os}}$  and  $v_{2,\text{ss}}$  in Fig. 4. This is presumably because of cancellation of the inaccuracies in  $v_{2,\text{os}}$  and  $v_{2,\text{ss}}$  caused by the approximations.

The behavior of  $\Delta v_{2,\text{pair}}$  is reminiscent of the  $\Delta\gamma$  observable [9] which is also composed of both CME signal and background and CME signal part is also quadratic in  $n_5/s$ . This is not surprising because the  $\Delta v_{2,\text{pair}}$  observable is effectively as same as the  $\Delta\gamma$  observable, with the arithmetic average angle  $(\phi_\alpha + \phi_\beta)/2$  replaced by the “ $p_T$ -weighted” one. For comparison, we plot  $\Delta\gamma$  in Fig. 7 in filled squares, also with a quadratic fit.

The three quantities,  $\Delta\gamma$ ,  $\Delta v_{2,\text{pair}}$ , and  $\Delta\gamma - v_{2,\pi}\Delta\delta$ ,

are all sensitive to the CME but are also all vulnerable to backgrounds. It appears that  $\Delta v_{2,\text{pair}}$  and  $\Delta\gamma - v_{2,\pi}\Delta\delta$  may have a smaller background contribution than  $\Delta\gamma$  has, presumably because of partial cancellations of backgrounds in  $\Delta\gamma$  and  $\Delta\delta$ . One may even consider the quantity  $\Delta\gamma - \kappa v_{2,\pi}\Delta\delta$  with a  $\kappa > 1$  parameter [16] to remove more background. However, the background contributions cannot be calculated a priori but have to be determined from data. Thus, all these observables are similar and have qualitatively the same sensitivities to the CME signal and background.

## V. SUMMARY

We have investigated, using the AVFD model, effects of the chiral magnetic effect (CME) on opposite-sign (OS) and same-sign (SS) pair-wise elliptic anisotropies, particularly on their difference  $\Delta v_{2,\text{pair}} \equiv v_{2,\text{os}} - v_{2,\text{ss}}$ . It is found that  $\Delta v_{2,\text{pair}}$  increases quadratically with increasing axial current density  $n_5/s$ , as expected. It is also found that the  $\Delta v_{2,\text{pair}}$  contains a background contribution. The CME signal and background in  $\Delta v_{2,\text{pair}}$  are also difficult to separate, similar to those in the charge-dependent azimuthal correlator  $\Delta\gamma$  observable. We conclude that the sensitivities of  $\Delta v_{2,\text{pair}}$  and  $\Delta\gamma$  (and  $\Delta\gamma - v_{2,\pi}\Delta\delta$ ) to the CME and background are similar, and the  $\Delta v_{2,\text{pair}}$  observable probably does not bring in significantly additional insights beyond the  $\Delta\gamma$  observable.

We have also studied resonance elliptic anisotropies ( $v_{2,\text{res}}$ ) as a function of  $n_5/s$ . While there may be potential contribution from the CME to  $v_{2,\text{res}}$ , it does not seem obvious and statistically significant to gain additional insights on the CME from resonance  $v_{2,\text{res}}$ .

## ACKNOWLEDGMENTS

We thank Dr. Jinfeng Liao and Dr. Gang Wang for useful discussions. This work was supported in part by the U.S. Department of Energy (Grant No. DE-SC0012910).

- 
- [1] D. Kharzeev, R. Pisarski, and M. H. Tytgat, Possibility of spontaneous parity violation in hot QCD, *Phys.Rev.Lett.* **81**, 512 (1998), arXiv:hep-ph/9804221 [hep-ph].
  - [2] D. Kharzeev, Parity violation in hot QCD: Why it can happen, and how to look for it, *Phys.Lett.* **B633**, 260 (2006), arXiv:hep-ph/0406125 [hep-ph].
  - [3] D. E. Kharzeev, L. D. McLerran, and H. J. Warringa, The Effects of topological charge change in heavy ion collisions: ‘Event by event P and CP violation’, *Nucl.Phys.* **A803**, 227 (2008), arXiv:0711.0950 [hep-ph].
  - [4] K. Fukushima, D. E. Kharzeev, and H. J. Warringa, The chiral magnetic effect, *Phys.Rev.* **D78**, 074033 (2008), arXiv:0808.3382 [hep-ph].
  - [5] V. Skokov, A. Yu. Illarionov, and V. Toneev, Estimate of the magnetic field strength in heavy-ion collisions, *Int. J. Mod. Phys.* **A24**, 5925 (2009), arXiv:0907.1396 [nucl-th].
  - [6] W.-T. Deng and X.-G. Huang, Event-by-event generation of electromagnetic fields in heavy-ion collisions, *Phys. Rev.* **C85**, 044907 (2012), arXiv:1201.5108 [nucl-th].
  - [7] D. E. Kharzeev, J. Liao, S. A. Voloshin, and G. Wang, Chiral magnetic and vortical effects in high-energy nuclear collisions—A status report, *Prog. Part. Nucl. Phys.* **88**, 1 (2016), arXiv:1511.04050 [hep-ph].
  - [8] J. Zhao and F. Wang, Experimental searches for the chiral magnetic effect in heavy-ion collisions, *Prog. Part. Nucl. Phys.* **107**, 200 (2019), arXiv:1906.11413 [nucl-ex].

- [9] S. A. Voloshin, Parity violation in hot QCD: How to detect it, *Phys.Rev.* **C70**, 057901 (2004), [arXiv:hep-ph/0406311 \[hep-ph\]](#).
- [10] F. Wang, Effects of Cluster Particle Correlations on Local Parity Violation Observables, *Phys.Rev.* **C81**, 064902 (2010), [arXiv:0911.1482 \[nucl-ex\]](#).
- [11] J. Liao, V. Koch, and A. Bzdak, On the Charge Separation Effect in Relativistic Heavy Ion Collisions, *Phys.Rev.* **C82**, 054902 (2010), [arXiv:1005.5380 \[nucl-th\]](#).
- [12] S. Schlichting and S. Pratt, Charge conservation at energies available at the BNL Relativistic Heavy Ion Collider and contributions to local parity violation observables, *Phys.Rev.* **C83**, 014913 (2011), [arXiv:1009.4283 \[nucl-th\]](#).
- [13] B. Abelev *et al.* (STAR Collaboration), Azimuthal Charged-Particle Correlations and Possible Local Strong Parity Violation, *Phys.Rev.Lett.* **103**, 251601 (2009), [arXiv:0909.1739 \[nucl-ex\]](#).
- [14] B. Abelev *et al.* (STAR Collaboration), Observation of charge-dependent azimuthal correlations and possible local strong parity violation in heavy ion collisions, *Phys.Rev.* **C81**, 054908 (2010), [arXiv:0909.1717 \[nucl-ex\]](#).
- [15] L. Adamczyk *et al.* (STAR), Measurement of charge multiplicity asymmetry correlations in high-energy nucleus-nucleus collisions at  $\sqrt{s_{NN}} = 200$  GeV, *Phys. Rev.* **C89**, 044908 (2014), [arXiv:1303.0901 \[nucl-ex\]](#).
- [16] L. Adamczyk *et al.* (STAR), Beam-energy dependence of charge separation along the magnetic field in Au+Au collisions at RHIC, *Phys. Rev. Lett.* **113**, 052302 (2014), [arXiv:1404.1433 \[nucl-ex\]](#).
- [17] V. Khachatryan *et al.* (CMS), Observation of charge-dependent azimuthal correlations in  $p$ -Pb collisions and its implication for the search for the chiral magnetic effect, *Phys. Rev. Lett.* **118**, 122301 (2017), [arXiv:1610.00263 \[nucl-ex\]](#).
- [18] S. Acharya *et al.* (ALICE), Constraining the magnitude of the Chiral Magnetic Effect with Event Shape Engineering in Pb-Pb collisions at  $\sqrt{s_{NN}} = 2.76$  TeV, *Phys. Lett.* **B777**, 151 (2018), [arXiv:1709.04723 \[nucl-ex\]](#).
- [19] J. Adam *et al.* (STAR), Charge-dependent pair correlations relative to a third particle in  $p + Au$  and  $d + Au$  collisions at RHIC, *Phys. Lett.* **B798**, 134975 (2019), [arXiv:1906.03373 \[nucl-ex\]](#).
- [20] H.-J. Xu, J. Zhao, X. Wang, H. Li, Z.-W. Lin, C. Shen, and F. Wang, Varying the chiral magnetic effect relative to flow in a single nucleus-nucleus collision, *Chin. Phys.* **C42**, 084103 (2018), [arXiv:1710.07265 \[nucl-th\]](#).
- [21] S. A. Voloshin, Estimate of the signal from the chiral magnetic effect in heavy-ion collisions from measurements relative to the participant and spectator flow planes, *Phys. Rev.* **C98**, 054911 (2018), [arXiv:1805.05300 \[nucl-ex\]](#).
- [22] M. Abdallah *et al.* (STAR), Search for the Chiral Magnetic Effect via Charge-Dependent Azimuthal Correlations Relative to Spectator and Participant Planes in Au+Au Collisions at  $\sqrt{s_{NN}} = 200$  GeV, *Phys. Rev. Lett.* **128**, 092301 (2022), [arXiv:2106.09243 \[nucl-ex\]](#).
- [23] A. Tang, Probe Chiral Magnetic Effect with Signed Balance Function, *Chin. Phys. C* **44**, 054101 (2020), [arXiv:1903.04622 \[nucl-ex\]](#).
- [24] Z. Xu, B. Chan, G. Wang, A. Tang, and H. Z. Huang, Event shape selection method in search of the chiral magnetic effect in heavy-ion collisions, *Phys. Lett. B* **848**, 138367 (2024), [arXiv:2307.14997 \[nucl-th\]](#).
- [25] S. Shi, Y. Jiang, E. Lilleskov, and J. Liao, Anomalous Chiral Transport in Heavy Ion Collisions from Anomalous-Viscous Fluid Dynamics, *Annals Phys.* **394**, 50 (2018), [arXiv:1711.02496 \[nucl-th\]](#).
- [26] Y. Jiang, S. Shi, Y. Yin, and J. Liao, Quantifying the chiral magnetic effect from anomalous-viscous fluid dynamics, *Chin. Phys. C* **42**, 011001 (2018), [arXiv:1611.04586 \[nucl-th\]](#).
- [27] S. Shi, H. Zhang, D. Hou, and J. Liao, Signatures of Chiral Magnetic Effect in the Collisions of Isobars, *Phys. Rev. Lett.* **125**, 242301 (2020), [arXiv:1910.14010 \[nucl-th\]](#).
- [28] U. W. Heinz and J. Liu, Pre-equilibrium dynamics and heavy-ion observables, *Nucl. Phys. A* **956**, 549 (2016), [arXiv:1512.08276 \[nucl-th\]](#).
- [29] J. Błoczynski, X.-G. Huang, X. Zhang, and J. Liao, Azimuthally fluctuating magnetic field and its impacts on observables in heavy-ion collisions, *Phys.Lett.* **B718**, 1529 (2013), [arXiv:1209.6594 \[nucl-th\]](#).
- [30] S. Choudhury *et al.*, Investigation of experimental observables in search of the chiral magnetic effect in heavy-ion collisions in the STAR experiment, *Chin. Phys. C* **46**, 014101 (2022), [arXiv:2105.06044 \[nucl-ex\]](#).
- [31] K. Ackermann *et al.* (STAR Collaboration), STAR detector overview, *Nucl.Instrum.Meth.* **A499**, 624 (2003).
- [32] B. I. Abelev *et al.* (STAR), Centrality dependence of charged hadron and strange hadron elliptic flow from  $\sqrt{s_{NN}} = 200$ -GeV Au + Au collisions, *Phys. Rev.* **C77**, 054901 (2008), [arXiv:0801.3466 \[nucl-ex\]](#).